

DISCONTINUOUS APPROACH FOR MESO-SCALE MODELING OF POROUS MATERIALS LIKE CONCRETE UNDER HIGH TEMPERATURE

GUILLERMO ETSE^{*}, DIEGO SAID SCHICCHI[†], ANTONIO CAGGIANO^{*} AND
MARIANELA RIPANI^{*}

^{*} CONICET and University of Buenos Aires, Argentina

e-mails: getse@herrera.unt.edu.ar, acaggiano@fi.uba.ar, mripani@fi.uba.ar

[†] Stiftung Institut für Werkstofftechnik, Bremen, Germany

and Instituto Nacional de Tecnología Industrial (INTI), Buenos Aires, Argentina

e-mail: schicchi@iwt.uni-bremen.de

Keywords: High Temperature, Cohesive fracture, Spalling, Meso-Scale, Porosity, Pore pressure.

Abstract: In this work, the failure behavior of concrete exposed to elevated temperatures is analyzed. A thermo-mechanical and poropressure-based interface model for failure analysis of concrete subjected to high temperature is presented. The model represents an extension of a fracture energy-based interface formulation to account for the damage induced by high temperatures and for the temperature dependent pore pressure and humidity in concrete. Thereby, the non-linear response of the proposed coupled thermo-mechanical interface model for porous materials like concrete is activated under kinematic and/or temperature and/or hydraulic increments (with or without jumps). A simplified procedure is proposed to account for the temperature dependent pore pressure in concrete. This contribution focuses on both the formulation of the novel interface constitutive theory and on the strategy proposed for mesoscopic finite element analysis of concrete failure behavior under different hydro-thermo-mechanical conditions. Finally, some numerical analysis are presented which demonstrated the predictive capabilities of the proposed interface model.

1 INTRODUCTION

The action of high temperature in concrete is a field of much interest and attention due to its crucial influence in strength, durability and serviceability conditions of structural components. As a matter of fact, long-term exposures to high temperature fields and fire strongly affect the most relevant thermo-mechanical properties of concrete materials such as cohesion, friction, stiffness and strength [1-2].

The exposure to high temperature and/or fire is one of the most destructive events that concrete buildings and structures may suffer [3-4]. The chemical composition, the physical

micro- and meso-structure as well as the moisture content and porosity of concrete drastically change under elevated temperatures [5-6]. The cause of such modifications is represented by the dehydration of the hardened cement paste and the conversion of calcium hydroxide into calcium oxide [7]. As a consequence, during and after long term exposure to high temperature, the most important mechanical features of concrete can adversely be affected. Experimental evidences demonstrate the dramatic and substantial changes of cohesion, tensile and compressive strengths as well as the Young modulus and Poisson's ratio of concrete due to the long term exposure to fire and/or high temperature [8-9].

When temperature rises, concrete loses weight with a progressive increase of its porosity. Particularly, from 20°C to 200°C cement-based materials quickly lose their specific weight as a result of evaporable water loss. Then, when temperature reaches the range between 200°C and 600°C the weight loss starts to be slower. This process is due to the dehydration of cement paste which deals with the loss of water, chemically combined to the calcium silicate hydrates. After 600 °C the decomposition of magnesium and calcium carbonates, which form part of the concrete matrix, produces further loss of weight which can reach the 10% of the total one [10-12].

Plenty of studies addressed the change of concrete mechanical properties when subjected to high temperature, with special focus on its durability. The study of the pore size distribution in concrete exposed to thermal action (up to 800°C) has been addressed by Janotka and Bagel [13]. This research confirmed that under increasing temperatures the pore size mainly grows and its distribution becomes more and more homogeneous. Porosity of concrete subjected to high temperatures may increase up to 40% of its initial value. It is worth mentioning that porosity rise is not only due to the evaporable water loss, but also to the dehydration of the gel structure formed by the calcium-silicate hydration products when concrete is exposed to elevated temperature [14].

One of the more interesting and crucial phenomena in concrete components when subjected to fire or high temperature is the so-called “spalling”. Such a phenomenon has been studied in literature from both the experimental [15-16] and theoretical [17-18] point of view. The process of spalling is quite complex, however the literature on this matter states that spalling of concrete mainly depends on the porosity of the cement matrix, the amount of water content and the stress state either due to thermal gradients and/or applied mechanical loads. During heating, the water within the concrete is transformed into steam and tends to migrate to colder areas of the concrete matrix. Once the vapor flux reaches coldest zones, it condenses again, forming a

fully saturated water layer. This process typically occurs in the neighborhood of the heated surface inside the concrete piece. This area is commonly called “moisture clog” and is characterized by a low permeability, generating an impermeable barrier to gases passage. Then, the continuous rise of temperature, with the subsequent generation of further vapor gases which cannot escape to colder areas due to the presence of the water barrier, generates pore pressure. Such increment in the pore pressure, added to the stresses induced by thermal strains, mainly activates the process of spalling. It is important to remark that pore pressure acts as a triggering of spalling phenomenon. Once the cracking process starts the pore pressure is quickly dissipated and the further development of spalling does only depends on the thermal stresses increments [5,19,20].

This paper presents a discrete-crack modeling approach aimed at reproducing and predicting the failure behavior of porous materials like concrete when subjected to high temperature fields. In this framework, a zero-thickness interface constitutive theory for porous media like concrete under high temperatures is presented, which is an extension of the temperature independent interface model for non-porous materials by Carol et al. [21]. This interface model deals with a novel pressure-dependent dehydration rule accounting for the porosity features of concrete and thermal conditions. The proposed interface model, as shown in this work, allows accurate mesoscopic simulations of concrete cracking and spalling when exposed to fire.

2 COUPLED THERMO-PORO-ELASTIC CONTINUOUS MODEL

The mechanics of porous media provides a useful theoretical framework for the study of transport problems in porous materials as concrete, soils and rocks. In this framework, porous media can be interpreted as multiphase materials composed by a deformable skeleton and pores with one or more saturating fluids.

2.1 Constitutive equations of thermo-poro-elastic materials

The constitutive equations of thermo-poro-elastic materials, in terms of total stress $\boldsymbol{\sigma}$, porosity evolution ϕ^e and vapor pore pressure p_{vp} , are described by means of the following equations [22]:

$$\begin{aligned}\boldsymbol{\sigma} &= \mathbf{C} : \boldsymbol{\varepsilon}^e - \mathbf{B} p_{vp} - \theta \mathbf{A} \\ \phi^e &= \mathbf{B} : \boldsymbol{\varepsilon}^e + \frac{1}{M} p_{vp} - \aleph \theta\end{aligned}\quad (1)$$

being \mathbf{C} the fourth order elastic tensor, $\boldsymbol{\varepsilon}^e$ the elastic strain tensor, $\mathbf{B} = b\mathbf{I}$ the Biot's tensor (being b the Biot's coefficient) and \mathbf{I} the second order identity tensor. Moreover, $\theta = T - T_0$ is the temperature rise (being T and T_0 the actual and reference temperatures, respectively), $\mathbf{A} = \alpha_\theta \mathbf{I}$ the thermal expansion tensor with α_θ the thermal coefficient, M is the Biot's modulus and, finally, \aleph is the latent heat of porosity variation.

2.2 Temperature-dependent properties

The elastic properties of concrete play a key role in its overall temperature dependent response. Based on several experimental results [23-25] the dependency of the concrete elasticity modulus E and of the Poisson's ratio ν on the temperature rise can be approximated by means of the following functions:

$$E = E_0 (1 - \alpha_E \theta) \quad (2)$$

$$\nu = \nu_0 (1 - \alpha_\nu \theta) \quad (3)$$

where E_0 and ν_0 are the elastic modulus and Poisson's ratio at T_0 , respectively, α_E and α_ν are degradation parameters to be calibrated (suggested values by the authors for normal strength concrete are $\alpha_E = 0.0014$ and $\alpha_\nu = 0.0010$).

Then, the Biot's coefficient and modulus depend on the temperature level and can be defined as [26]:

$$b = \begin{cases} b_{min}, & T < T_{b1}, \\ \frac{1}{2} \left\{ (1 - b_{min}) \sin[\alpha_b] + (1 + b_{min}) \right\}, & \\ 1, & T > T_{b2}. \end{cases} \quad (4)$$

$$\text{with } \alpha_b = \frac{T - T_{b1}}{T_{b2} - T_{b1}} \pi - \frac{\pi}{2}$$

$$M = \begin{cases} M_0, & T < T_{tr}, \\ \frac{1}{2} \left\{ \Delta M \sin[\alpha_M] + \Delta M \right\}, & \\ M_{res}, & T > T_{res}. \end{cases} \quad (5)$$

$$\text{with } \alpha_M = \frac{\theta}{T_{tr} - T_0} \pi - \frac{\pi}{2}$$

$$\Delta M = M_0 - M_{res}$$

being T_{b1} , T_{b2} , T_{tr} and T_{res} (temperature) parameters to be calibrated. Suggested values are $T_{b1} = 100^\circ\text{C}$, $T_{b2} = 500^\circ\text{C}$ and $T_{tr} = 200^\circ\text{C}$ (this latter represents the trigger temperature when spalling starts).

The Biot's coefficient b ranges between its minimum value b_{min} at T_{b1} and its maximum one $b_{max} = 1$ when $T \geq T_{b2}$. On the other hand, the Biot's modulus M decreases from its maximum value M_0 at T_{tr} up to its minimum one, M_{res} , at $T_{res} = 2T_{tr} - T_0$.

3 COUPLED THERMO-PORO-PLASTIC DISCONTINUOUS MODEL

This section reports the temperature dependent interface formulation aimed at analyzing cracking behavior of quasi-brittle porous materials such as cementitious mortar and concrete.

Stresses and relative displacements are defined at the discontinuity mid-plane of each interface. The principle of "effective stresses" applied to the particular case of discontinuities considers that the fluid pressure influences the normal stress component (i.e., similar to the volumetric component in the continuum formulation, see Eq. 1).

Thus, following the formulation by Segura and Carol [27]:

$$\bar{\mathbf{t}} = \mathbf{t} + \alpha_j \mathbf{b} p_{vp} \quad (6)$$

where $\bar{\mathbf{t}} = [\bar{\sigma}_N, \sigma_T]^t$ and $\mathbf{t} = [\sigma_N, \sigma_T]^t$ are the mid-plane effective and total stress vectors, respectively, $\bar{\sigma}_N$ and σ_N are the effective and total normal stresses, σ_T is the shear stress component, α_j the discontinuity Biot's coefficient [28] and $\mathbf{b} = [1, 0]^t$ is a vector that introduces the influence of the fluid pore-pressure acting in the normal direction to the discontinuity axis.

The basic constitutive equations of the proposed elasto-thermo-poroplastic interface model are the following [29]:

$$\begin{aligned} \dot{\mathbf{u}} &= \dot{\mathbf{u}}^{el} + \dot{\mathbf{u}}^{cr} + \dot{\mathbf{u}}^{th} \\ \dot{\mathbf{u}}^{el} &= \mathbf{C}_a^{-1} \cdot \dot{\bar{\mathbf{t}}} \\ \dot{\bar{\mathbf{t}}} &= \mathbf{C}_a \cdot (\dot{\mathbf{u}} - \dot{\mathbf{u}}^{cr} - \dot{\mathbf{u}}^{th}) \end{aligned} \quad (7)$$

where $\dot{\mathbf{u}} = [\dot{u}, \dot{v}]^t$ is the vector of the relative displacement rates across the interface, which is additively decomposed into the elastic, plastic and thermal components, $\dot{\mathbf{u}}^{el}$, $\dot{\mathbf{u}}^{cr}$ and $\dot{\mathbf{u}}^{th}$, respectively; $\dot{\bar{\mathbf{t}}} = [\dot{\bar{\sigma}}_N, \dot{\sigma}_T]^t$ is the effective stress rate vector defined in the normal and tangential interface directions. Moreover, \mathbf{C}_a defines the elastic stiffness matrix, thermally degraded through the temperature-based scalar variable, d_τ :

$$\mathbf{C}_a = d_\tau \mathbf{C} \quad \text{with} \quad \mathbf{C} = \begin{pmatrix} k_N & 0 \\ 0 & k_T \end{pmatrix} \quad (8)$$

where k_N and k_T are the interface normal and tangential elastic stiffness, respectively.

The rate of normal and tangential interface effective stresses can be derived through the rates of relative displacement vector and temperature rise as:

$$\dot{\bar{\mathbf{t}}} = \mathbf{C}_a^{ep} \cdot \dot{\mathbf{u}} - \bar{\mathbf{f}}[\dot{T}] \quad (9)$$

being \mathbf{C}_a^{ep} the tangential interface stiffness for elastic degradation while $\bar{\mathbf{f}}[\dot{T}]$ the thermal interface effective stresses due to the rate of interface temperature field.

The complete formulation of the elasto-thermo-plastic rate equations which can be derived from the description of the thermal and plastic interface displacements, the formulation of a temperature dependent yield criterion, the adoption of temperature and fracture-energy dependent evolution laws are omitted in this work for the sake of brevity. A detailed formulation was published by the authors in [29].

4 VAPOR PRESSURE

As previously described in the introduction, due to the moisture evaporation phenomena, the relative humidity of concrete in the heated surface zones tends to decrease to very low values. Consequently a sharp front, separating the moist and dry material, moves inwards and at this "impermeable" front, an intensive evaporation process tries to take place, increasing considerably the so-called vapor pressure. The variation of the pore pressure in concrete with the temperature was experimentally measured by Pereira et al. [30].

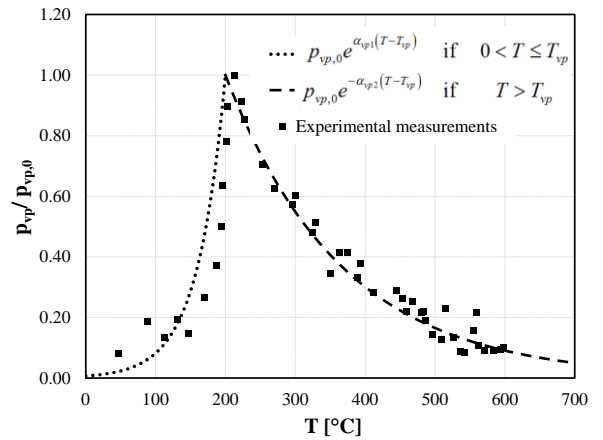


Figure 1: p_{vp} – temperature rule: comparison of the proposed law against poropressure measurements at 20 mm from the heating surface by Pereira et al. [30].

In this work, a simplified procedure to account for the vapor pressure in both continuous and discontinuous models detailed in Sections 2 and 3 is proposed. Particularly, the following expressions have been employed for the pore pressure evolution:

$$p_{vp} = \begin{cases} 0 & \text{if } T \leq 0 \\ p_{vp,0} e^{\alpha_{vp1}(T-T_{vp})} & \text{if } 0 < T \leq T_{vp} \\ p_{vp,0} e^{-\alpha_{vp2}(T-T_{vp})} & \text{if } T > T_{vp} \end{cases} \quad (10)$$

where $p_{vp,0}$, T_{vp} , α_{vp1} and α_{vp2} are model parameters to be calibrated. Figure 1 shows the plot of the p_{vp} -temperature rule and, as an example, a comparison of the considered law against pore pressure measurements at a depth of 20 mm from the heating surface of a concrete specimen by Pereira et al. [30] is reported.

It is worth mentioning that the classical way for modeling drying processes and vapor diffusion phenomena in porous media like concrete deals with calculating the moisture diffusion which takes place in its porous structure. This can be approached by means of modeling the migration of the “evaporable water” throughout the pore structure of the cementitious composite. Then, the vapor pore pressure should be computed as result of this complex phenomenon dealing with moisture and temperature diffusion phenomena coupled with mechanical effects induced by thermal events. This further development is out of the scopes of this work and it will be certainly considered by the authors in future work of this research line.

4 NUMERICAL ANALYSES

This section proposes some calibrations and numerical applications of the proposed model. For the calibration purpose, experimental results on concrete specimens tested under pure tension are considered. After this, failure processes in concrete under coupled temperature and fracture loading are taken into account for the evaluation of model predictive capabilities.

4.1 Interface model calibration

Tensile tests (Figure 2) performed on concrete specimens after being exposed to room, medium and high temperatures (at residual stages) are considered as a reference.

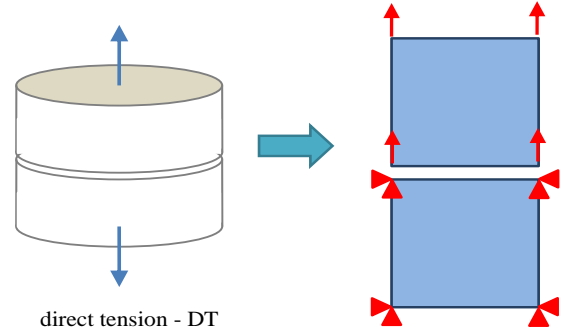


Figure 2: Test set-up of tensile tests.

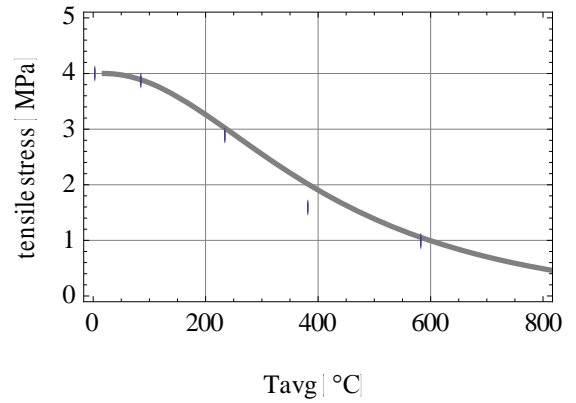


Figure 3: Strength decay in direct tensile tests: experimental results [31] and model predictions.

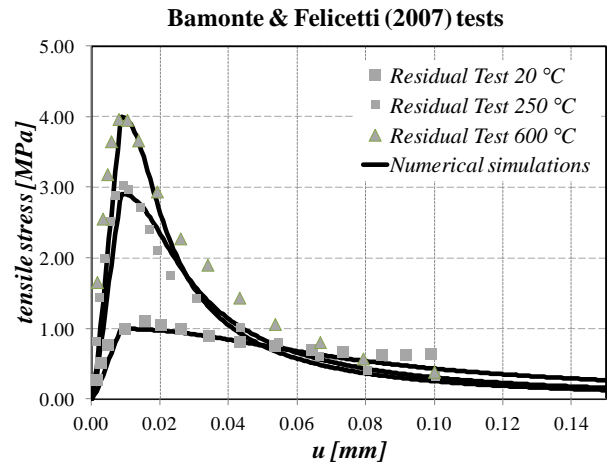


Figure 4: Residual stress-crack opening curves: experimental results [31] against numerical predictions.

For this purpose, experimental results presented by Bamonte and Felicetti [31] were considered. As a result of the calibration analysis [29], a decay trend occurred for both the concrete tensile strength and elastic stiffness. Experimental data exhibited a similar behavior against increasing temperatures. Particularly, Figure 3 deals with the variation

of concrete peak strength with temperature, obtained from the direct tensile tests by Bamonte and Felicetti [31] and those obtained with the numerical prediction based on the interface model parameters and its internal decay functions as indicated above.

Moreover, the comparison between the same experimental results and numerical data in terms of stresses vs. crack opening displacements, for three different temperature levels, is highlighted in Figure 4. Beyond the general soundness of the interface model predictions for failure behavior of concrete affected by temperature, the numerical results demonstrate the capabilities of the proposed formulation to reproduce the strong sensitivity of the concrete mechanical behavior on the acting temperature.

4.2 Pore-pressure coupled analysis

In this section, the predictions of the temperature-based interface model are evaluated under tensile loads and subjected to thermo-mechanical couplings with or without consideration of the pore pressure effects.

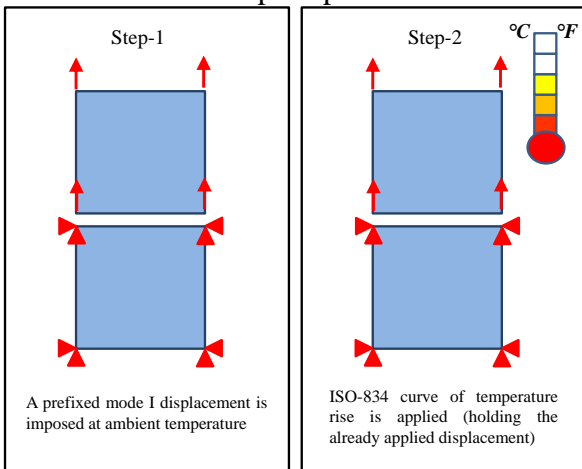


Figure 5: Specimen geometry, boundary conditions and considered steps.

The discontinuous model was previously calibrated with the experimental data of residual mechanical properties as proposed in Section 4.1, while the thermal parameters given in Table 1 were considered. Furthermore, the adopted poropressures are those highlighted in Figure 1.

Figure 6 shows the temperature-dependent behavior of a tensile test as predicted by the

proposed model. Particularly, Figure 6(a) shows the imposed displacement-temperature input in the tensile test. In the first step of the test, only mode I displacements are imposed, at room temperature (i.e., 20 °C). Then, in a second step of the test, the ISO-834 temperature curve is applied, while keeping constant the previously applied tensile displacement (similarly to the well-known relaxation test, see Figure 5).

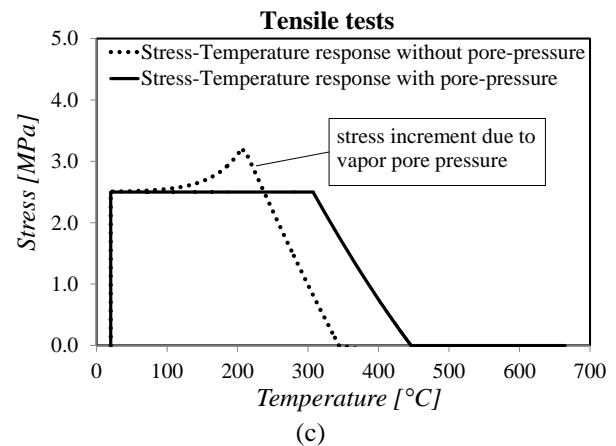
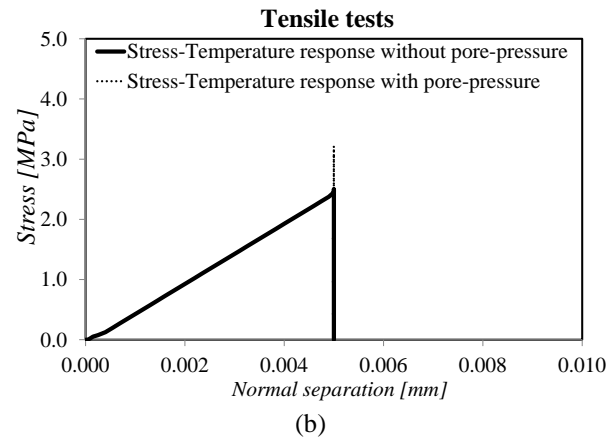
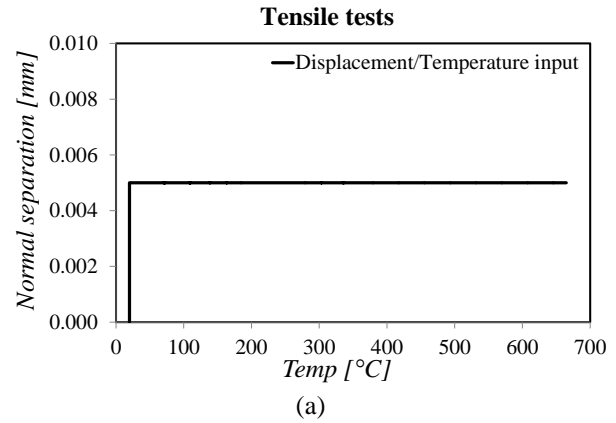


Figure 6: Stress-temperature behavior with and without poropressure: (a) displacement-temperature history, (b) normal stress vs. opening displacements and (c) stress-temperature response.

Table 1: Thermal parameters of concrete according to EN 1992-1-2:2004 [32].

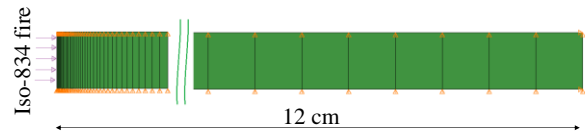
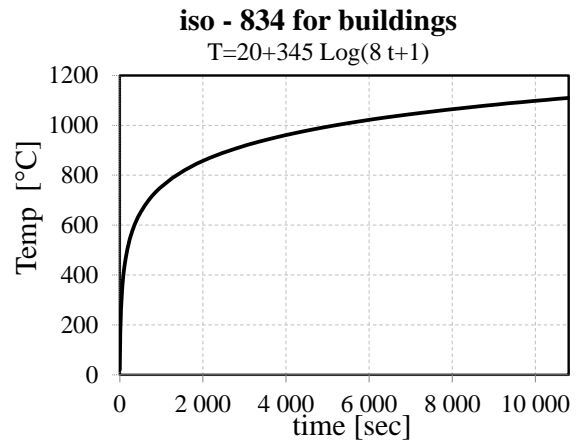
T [°C]	c_p [J kg ⁻¹ °C ⁻¹]	λ [W m ⁻¹ °C ⁻¹]	ε_{th} [-]
20	900	1.642218	1.12E-07
100	1470	1.49765	4.94E-04
200	1000	1.3317	1.19E-03
400	1100	1.049	3.18E-03
500	1100	0.93225	4.63E-03
600	1100	0.8319	6.50E-03
700	1100	0.74795	8.88E-03
734	1100	0.72314292	9.82E-03
800	1100	0.6804	1.18E-02
900	1100	0.62925	1.20E-02
1000	1100	0.5945	1.20E-02
1100	1100	0.57615	1.20E-02
1200	1100	0.5742	1.20E-02

T [°C]	ρ [kg/m ³]	E [GPa]	ν [-]
20	2300	3.82E+01	0.2
100	2300	33.9216	0.184
200	2254	28.5736	0.164
400	2185	17.8776	0.124
500	2.16E+03	12.5296	0.104
600	2.14E+03	7.1816	0.084
700	2.12E+03	1.8336	0.064
734	2.12E+03	0.01528	0.0572
800	2.10E+03	0.01528	0.0572
900	2.08E+03	0.01528	0.0572
1000	2.06E+03	0.01528	0.0572
1100	2.04E+03	0.01528	0.0572
1200	2.02E+03	0.01528	0.0572

Figure 6(b) and (c) illustrate the results in terms of normal stress-opening displacements and stress-temperature response, respectively, in case of considering (or not) the vapor pore pressure effects. Poropressure produces an increment of the effective normal stress, approaching the failure surface of the interface at a temperature of 209 °C (without poropressure it is reached at 310 °C). Then, the internal parameters, damaged through the temperature-based dehydration rule, softens the response of the specimen up to the complete failure (i.e., the tensile stress becomes null). When considering vapor poropressure, the numerical test shown in Figure 5, indicates that the failure state is reached at about 343 °C while without considering poropressure effects the process is slower and the total failure occurs at 446 °C.

4.3 Wall exposed on one side to the standard ISO fire curve

The description of physical phenomena in heated concrete walls presented in this section follows similar numerical tests available in scientific literature regarding high temperature tests of concrete elements [33-36]. Here, the results of simulations concerning a 12-cm wall (the same thermo-poro-mechanical parameters of Section 4.2 are considered), exposed on one side to the standard ISO-834 (Figure 7) are outlined. The heated surface generates a gradual increase of the element temperature, starting from the surface as illustrated in Figure 8. Due to that an empirical rule is adopted, the corresponding vapor pressure curves at different times are plotted in Figure 10. The maximum values of the vapor poropressure curves (0.7-0.8 MPa) coincide with the position where the temperature reaches approximately 200 °C.


Figure 7: Boundary examples for the simulation of a 12-cm wall during exposed to ISO-FIRE 834 heating.

Figure 8: The temperature development of the buildings fire curve, ISO-834.

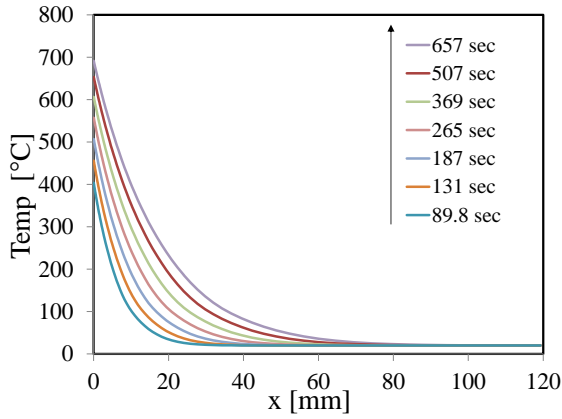


Figure 9: Temperature vs. abscissa X at several times.

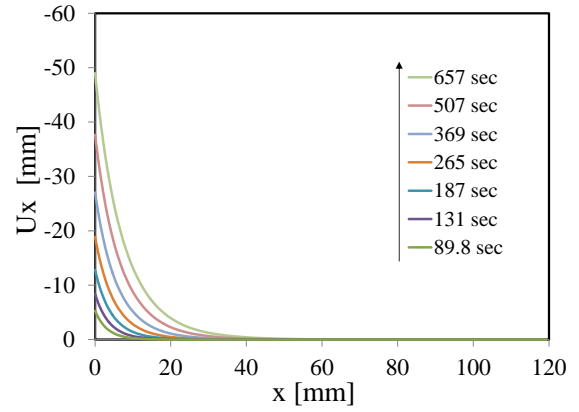


Figure 11: U_x displacement vs. abscissa X at several times.

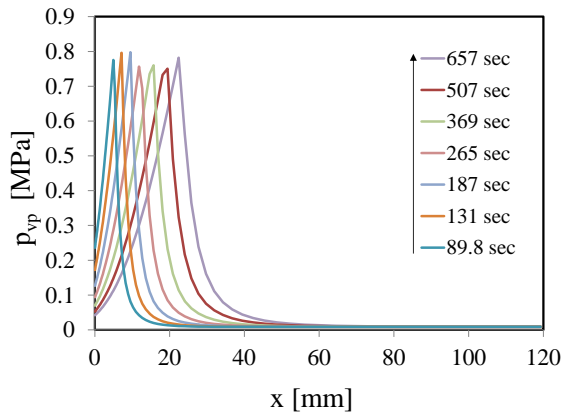


Figure 10: Pore-pressure vs. abscissa X at several times.

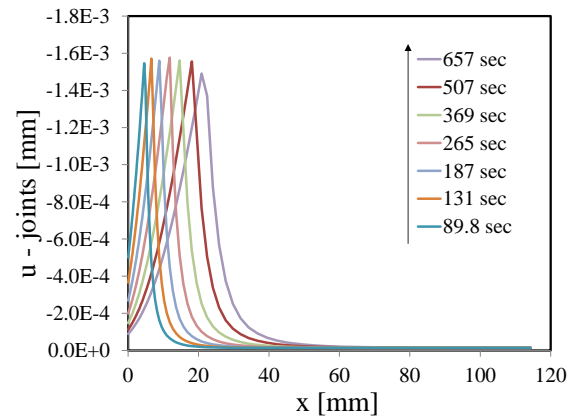


Figure 12: Interface opening displacement vs. abscissa X at several times.

Increasing temperature causes concrete material dilatations. Figure 11 highlights the U_x displacement response due to such thermal dilatation. However, this phenomenon can be in part caused to the classical thermal dilatation of the material, and, also can be caused by the progressive crack opening. Concrete cracking and spalling, during heating processes, is mainly caused by the thermal dilatation of the coarse aggregate which leads to high traction stresses in the Interface Transition Zones with the surrounding mortar and, consequently, to the development of local micro-cracks.

When cracks parallel to the heated surface starts to be formed, e.g., due to an external load or as result of constrained thermal dilatations of the surface layer and/or meso-scale components, the vapor pore pressure can contribute to the material spalling, and particularly to further increase of the interface jumps as demonstrated in Figure 12.

5 CONCLUDING REMARKS

This paper addressed the formulation of a novel coupled pore pressure-based and coupled thermo-mechanical interface model for porous materials like concrete when subjected to high temperatures. The principle of “effective stresses”, applied to the particular case of interface discontinuities was considered in conjunction with the influence of the fluid pressure on the normal total stress components. Particularly, this proposal took into account a quadratic hyperbola as a maximum strength criterion for the interface, defining the interaction between maximum shear and normal interface effective stresses. Consequently, the constitutive formulation explicitly considered the thermal effects and the vapor pore pressure into the failure criterion and the resulting post-cracking response through a temperature-based scaling function affecting the strength parameters and

the softening law. Numerical analyses, performed with the constitutive model presented in this paper, demonstrated its predictive capabilities in terms of the most relevant aspects of the mechanical behavior of concrete under high temperatures. The proposed interface model can also be employed in mesoscopic analyses using mortar-mortar and mortar-aggregate interfaces aimed at simulating failure processes and spalling phenomena of concrete specimens under high temperatures.

ACKNOWLEDGMENTS

The authors acknowledge the financial support for this work by the SUPERCONCRETE Project (H2020-MSCA-RISE-2014–n. 645704) funded by the European Union as part of the H2020 Programme.

REFERENCES

- [1] Gao, W.Y., Dai, J.G., Teng, J.G. and Chen, G.M. 2013. Finite element modeling of reinforced concrete beams exposed to fire. *Eng. Struct.* 52:488-501.
- [2] Gernay, T. and Franssen, J.M. 2015. A plastic-damage model for concrete in fire: Applications in structural fire engineering. *Fire Safety J.*, 71:268-278.
- [3] Ripani, M., Etse, G., Vrech, S. and Mroginski, J. 2014. Thermodynamic gradient-based poroplastic theory for concrete under high temperatures, *Int J Plasticity*, 61:157-177.
- [4] Mousavi, S., Bagchi, A. and Kodur, V.K. 2008. Review of post-earthquake fire hazard to building structures, *Canadian J Civil Engineering*, 35:689-698.
- [5] Gawin, D., Pesavento, F. and Schrefler, B. 2003. Modelling of hygro-thermal behaviour of concrete at high temperature with thermo-chemical and mechanical material degradation, *Comp Meth App Mech Engng*, 192: 1731-1771.
- [6] Bahr, O., Schaumann, P., Bollen, B. and Bracke, J. 2013. Young's modulus and Poisson's ratio of concrete at high temperatures: Exp. investigations, *Mat and Design*, 45:421-429.
- [7] Kizilkanat, A.B., Yuzeer, N. and Kabay, N. 2013. Thermo-physical properties of concrete exposed to high temperature, *Cons Build Materials*, 45: 157-161.
- [8] Tanyildizi, H. and Coskun, A. 2008. The effect of high temperature on compressive strength and splitting tensile strength of structural lightweight concrete containing fly ash, *Construct Building Materials*, 22:2269-2275.
- [9] Phan, L.T. and Carino, N.J. 2002. Effects of test conditions and mixture proportions on behavior of high-strength concrete exposed to high temperatures, *ACI Material J*, 99:54-66.
- [10] Lee, J., Xi, Y. And Willam, K. 2008. Properties of concrete after high-temperature heating and cooling. *ACI Mater. J.* 105:334-341.
- [11] Zhang, B. and Bicanic, N. 2002. Residual fracture toughness of normal- and high-strength gravel concrete after heating to 600C. *ACI Mat. J.* 99:217-226.
- [12] Zhang, B. 2011. Effects of moisture evaporation (weight loss) on fracture properties of high performance concrete subjected to high temperatures. *Fire Safety J.* 46:543-549.
- [13] Janotka, I. and Bagel, L. 2002. Pore structures, permeabilities, and compressive strengths of concrete at temperatures up to 800 C. *ACI Mater. J.* 100:196-200.
- [14] Harmathy, T.Z. 1970. Thermal Properties of Concrete at Elevated Temperature, *J. of Material* 5:47-74.
- [15] Kalifa, P. and Menneteau, F.D. and Quenard, D. 2000. Spalling and porepressure in HPC at high temperature, *Cem Concrete Research* 1:1915-1927.
- [16] Kalifa, P., Chene, G. and Galle, C. 2001. High-temperature behavior of HPC with polypropylene fibres: From spalling to microstructure, *Cement Concrete Research* 31(10):1487-1499.
- [17] Bazant, Z.P. 1997. Analysis of pore pressure, thermal stresses and fracture in

- rapidly heated concrete, *Int. Workshop on Fire Performance of High Strength Concrete 13-14, CD-ROM*.
- [18] Gawin, D. and Schrefler, B.A. 1996. Thermo-hydro-mechanical analysis of partially saturated porous materials, *Eng. Computations* 13(7):113-143.
- [19] Hager I. 2013. Behaviour of cement concrete at high temperature. *Bull. Pol. Ac.: Tech.* 61(1):1-10.
- [20] Schrefler, B.A., Gawin, D., Majorana, C.E., and Pesavento, F. 2001. FE analysis of thermo-hydro mechanical behaviour of concrete at high temperature. *Comput Mech - New Front for new millennium S.* pp. 827-836.
- [21] Carol, I., Prat, P. and Lopez, C. 1997. Normal/shear cracking model: applications to discrete crack analysis, *ASCE-J EngrgMech* 123:765-773.
- [22] Coussy, O., 2004. Poromechanics. *John Wiley & Sons*.
- [23] Chang, Y. F., Chen, Y. H., Sheu, M. S. and Yao, G.C. 2006. Residual stress-strain relationship for concrete after exposure to high temperatures. *Cement Concrete Res.* 36:1999-2005.
- [24] Guo, Z. and Shi, X. 2011. Experiment and Calculation of Reinforced Concrete at Elevated Temperatures, *1st edition. Ed. Butterworth-H. Waltham, USA*.
- [25] Bahr, O., Schaumann, P., Bollen, B. and Bracke, J. 2013. Young's modulus and Poisson's ratio of concrete at high temperatures: Experimental investigations. *Mater. Design* 45:421-429.
- [26] Zhang, Y., Zeiml, M., Pichler, C. and Lackner, R. 2014. Model-based risk assessment of concrete spalling in tunnel linings under fire loading. *Eng. Struct.* 77:207-215.
- [27] Segura, J.M. and Carol I. 2008. Coupled HM analysis using zero-thickness interface elements with double nodes. Part I: Theoretical model, *Int. J. Numer. Anal. Meth. Geomech.* 32:2083-2101.
- [28] Noorishad, J., Ayatollahi, M.S. and Witherspoon, P.A. 1982. A finite-element method for coupled stress and fluid flow analysis in fractured rock masses. *Int. J. of Rock Mechanics and Mining Science and Geomechanics Abstracts* 19:185-193.
- [29] Caggiano, A. and Etse, G. 2015. Coupled thermo-mechanical interface model for concrete failure analysis under high temperature. *Computer Methods in App Mech & Engineering* 289:498-516.
- [30] Pereira, F., Pistol, K., Korzen, M., Weise, F., Pimienta, P., Carré, H. and Huismann, S. 2011. Monitoring of fire damage processes in concrete by pore pressure and acoustic emission measurements. *2nd international Rilem workshop on concrete spalling due to fire exposure, Delft, The Netherlands (pp. 5-7)*.
- [31] Bamonte, P. and Felicetti, R. 2007. On the tensile behavior of thermally-damaged concrete. *In Proceedings of the 6th International Conference on Fracture Mechanics of Concrete and Concrete Structures*, Taylor & Francis, London, UK, pp.1715-1722.
- [32] EN 1992-1-2 2004. (English): *Eurocode 2: Design of concrete structures - Part 1-2: General rules - Structural fire design*.
- [33] Gawin, D., Majorana, C.E. and Schrefler, B.A. 1999. Numerical analysis of hygro-thermic behaviour and damage of concrete at high temperature, *Mech. Cohes.-Frict. Mater.* 4:37-74.
- [34] Gawin, D., Pesavento, F. and Schrefler, B.A. 2002. Simulation of damage-permeability coupling in hygro-thermo-mechanical analysis of concrete at high temperature, *Commun. Numer. Methods Engrg.* 18:113-119.
- [35] Gawin, D., Pesavento, F. and Schrefler, B.A. 2004. Modelling of deformations of high strength concrete at elevated temperatures, *Concr. Sci. Engrg./ Mater. Struct.* 37(268):218-236.
- [36] Khoury, G.A. 1995. Strain components of nuclear-reactor-type concretes during first heating cycle, *Nucl. Engrg. Des.* 156:313-321.